

SECOND SOUND MEASUREMENT FOR SPL CAVITY DIAGNOSTICS

K. Liao*, C. Balle, J. Bremer, T. Junginger, W. Vollenberg, W. Weingarten,
 CERN, Geneva, Switzerland,
 H. Vennekate[#], University of Göttingen, Germany

Abstract

Second sound is a temperature wave which travels at a speed of $\approx 20\text{m/s}$ in superfluid helium. The second sound detector used is a so-called oscillating superleak transducer (OST), initially provided by Cornell-CLASSE, and thereafter manufactured at CERN. It contains a flexible porous membrane for transmitting and blocking the movement of the superfluid and normal fluid components of the second sound wave. From the measured speed of this wave and by determining the travel time between the quench event and several OSTs, an alternative method is offered to localise the quench site by triangulation. Several surface mount devices (SMDs) – thick film chip resistors – are used to simulate the quench spot in a cavity. Given the heat pulse and the location of the installed OSTs, the temperature dependence of the second sound velocity is determined under different experimental conditions and compared with previous results and theoretical expectations. The second sound triangulation will eventually be used to determine quench locations on the Superconducting Proton Linac (SPL) test cavities (704MHz) at CERN.

INTRODUCTION

Second sound is a quantum mechanical phenomenon exhibited in superfluids. The name “second sound” is derived by analogy with first sound where the former propagates as an entropy wave and the latter, a density wave. The oscillating superleak transducer was developed and constructed by R. Sherlock and D. Edwards in the 1970s [1] to detect second sound in superfluid ^4He and in dilute ^3He - ^4He mixtures at few milli-Kelvin. The OST contains a superleak membrane with micrometer size pores which allow the movement of superfluid component go through without viscosity leaving the viscous normal fluid component outside. The oscillation of the two fluids introduces the principle of operation and the name of this second sound detector – oscillating superleak transducer. This technique was first introduced by K. W. Shepard [2] for the detection of the quench location in a superconducting cavity. Since then this technique has been widely used in second sound measurement in many laboratories over the last few decades and in quench detection in cavity diagnostics [3-7]. This paper reports on second sound characteristics for quench detection being studied in a dedicated cryostat in CERN’s Cryolab.

The paper is split into four parts. First, the experimental setup and procedure is introduced. Second, second sound measurement improvements and results of characteristics studies are presented. Third, the manufacturing process and membrane sputtering regarding OSTs at CERN are

described (with a slight change to Cornell’s design). Finally, the paper is distilled with some conclusive remarks and an outline of future plans.

EXPERIMENTAL SETUP

Six surface mount devices (SMDs) – thick film chip resistors with various specifications – are soldered on a printed circuit board with dimensions $20 \times 10 \times 1.5 \text{ mm}^3$ (Table 1). One side of the board has printed circuitry while the other one remains insulated so to be fixed on the bottom plate of the insert (see Fig.1 (a)).

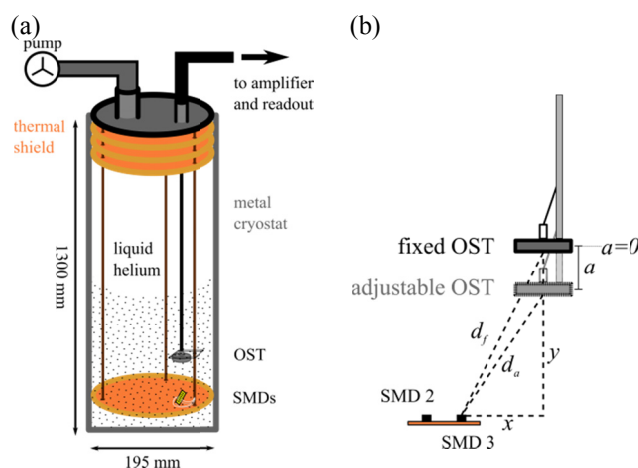


Figure 1: (a) Illustration of the experimental setup. (b) The orientation of the two OSTs. The distances between the SMDs and the OSTs are determined by the fixed x , y values and the increment a or decrement $-a$ on the adjustable insert.

One oscillating superleak transducer (OST) was mounted at a fixed distance of d_f above the SMD board where the level is defined as $a = 0$ (see Fig.1 (b)). A second OST is mounted on a movable rod on the insert which is manually adjustable. Thus the distance between the OST and the SMD used is determined by the Pythagoras’ theorem. The distance is measured by a ruler with a measurement error of $\pm 1 \text{ mm}$ in both the x and y direction. Temperature is monitored by one Cernox sensor (Lakeshore CX-1050-SD-1.4L) and the signal is read out via a Labview programme. The insert is to be fitted in a metal cryostat filled with liquid ^4He .

Measurement Procedure

The pulse technique is used to trigger the SMDs on the board in order to initiate the second sound wave (see Fig. 2). The second sound signal received from the OST is amplified by 23 times and displayed on the oscilloscope (Tektronix MSO/DPO 3000 series). The amplifier box

* kitty.liao@cern.ch

[#]Technical Student at CERN

contains an amplifier circuit and is equipped with two switches (battery or power supply) as the 120 V charger for the OST and the 12 V amplifier charger.

Table 1: Selected SMD resistors [8]

SMD	R (Ω) at 300K	Power specification (W)	Measured R at 1.7K (Ω)
1	20	1/8	25.4 ± 0.0005
2	51	1/10	63.7 ± 0.0005
3	51	1/8	66.9 ± 0.0005
4	110	1/8	153.3 ± 0.0005
5	300	1/10	370.2 ± 0.0005
6	1k	1/4	$1.49k \pm 0.0005$

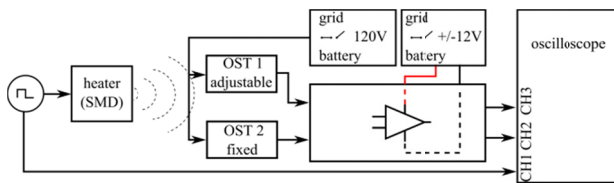


Figure 2: Measurement procedure.

SECOND SOUND MEASUREMENT

Noise Reduction

The noise along with the second sound signals measured in a metal cryostat connected to the building ground is shown in Fig. 3. To eliminate the major 50 Hz hum the building ground connection was removed (see Fig. 4(a)), and this was done by adding a paper carton between the Cryolab ground and a plastic joint between the pump line and the cryostat.

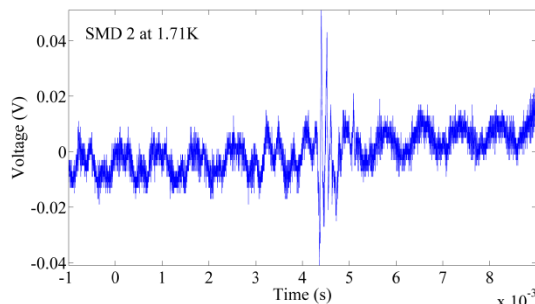


Figure 3: Second sound signal before noise reduction. The signal is triggered by a 10 V, 0.2 ms pulse on SMD 2 (62 Ω) at 1.71 K which shows a noise level of ≈ 30 mV_{peak-peak}.

The noise coming from the 120 V power supply for the OST was then discernible after the elimination of the 50 Hz (see Fig. 4(b)). The 120 V battery option then lowered the noise level to ≈ 1 mV. The ± 15 V battery option however did not provide prominent noise reduction to the ± 12 V power supply for the amplifier circuit. As a result, the noise level is reduced by 53% (see Fig. 3 and Fig. 5).

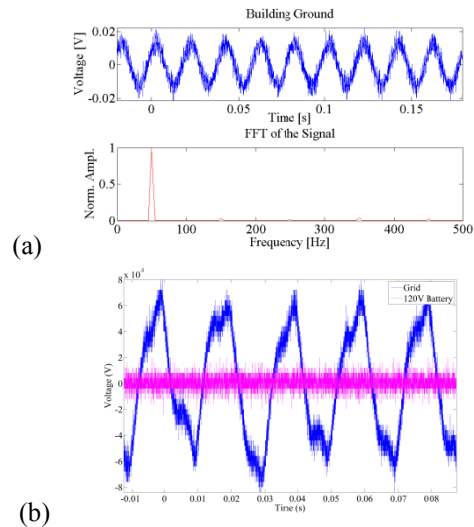


Figure 4: (a) The noise presented from the building ground and its Fast Fourier Transform (FFT). (b) 120 V power supply from the grid for the OST and the signal when it is switched to the battery.

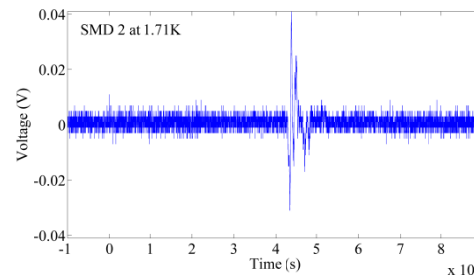


Figure 5: Second sound signal after noise reduction. The signal is triggered by a 10 V, 0.2ms pulse on SMD 2 (62 Ω) at 1.71 K which shows a noise level of ≈ 14 mV_{peak-peak}.

Signal Characteristics

The six SMD resistors are tested one by one in order to select those which provide better signal-to-noise ratio (S/N) for our analysis, consequently SMD 2 and SMD 3 with 0.8 mm² and 1.63 mm² surface area, respectively, are used.

The 10 V maximum input pulse generated from the function generator is lowered at a fixed liquid helium temperature 1.69 K to test the OST response. A series of second sound signal amplitude versus input voltage is shown in Fig. 6. The second sound amplitude is no longer discernible at 1.5 V input as it dropped to 6.3 mV_{peak-peak}.

To extend the signal characteristics study, the second sound amplitude was measured below the lambda point (2.17 K) down to 1.5 K. The temperature error is within ± 4 mK quoted from the Cernox calibration sheet. The curve in Fig. 7 shows the trend of the second sound amplitude's decline while the helium temperature rises. The amplitude error is within ± 4.2 mV. It is then worthy of notice that the temperature under which a quench is detected affects the detection of the signal strength.

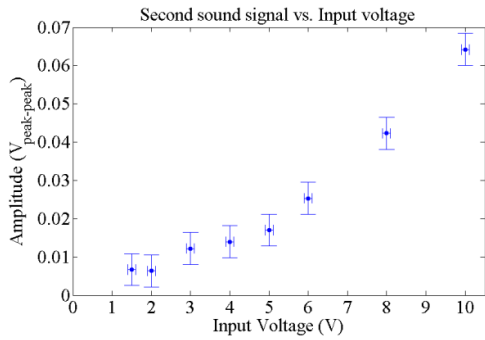


Figure 6: Second sound signal amplitude change according to different voltage input (0.2 ms input pulse on SMD 3).

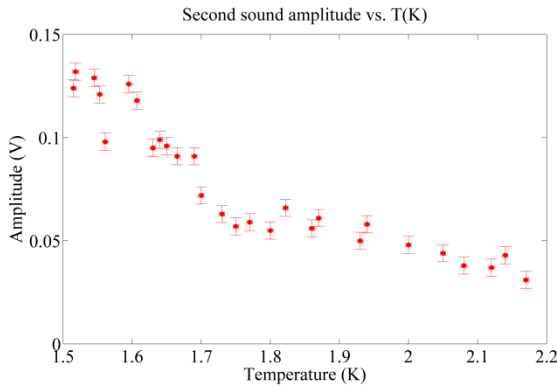


Figure 7: Second sound signal amplitude vs. temperature change (10 V, 0.2 ms input pulse on SMD 3).

Second Sound Velocity

The second sound velocity is given by,

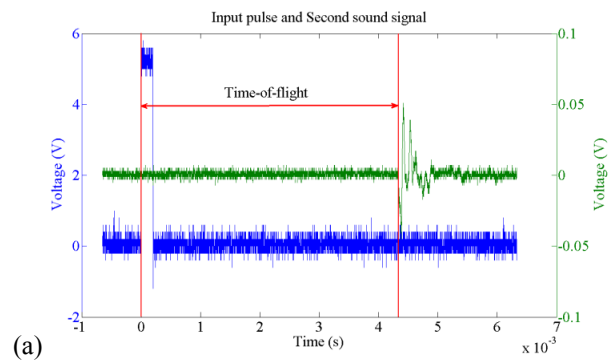
$$v^2 = \left(\frac{\rho}{\rho_n} - 1 \right) \frac{TS^2}{C_v} \quad (1) [9]$$

where ρ is the liquid helium density (g/cm^3), ρ_n the normal fluid density (g/cm^3), T the temperature (K), S the entropy ($\text{J/mole}\cdot\text{K}$), C_v the heat capacity ($\text{J/mole}\cdot\text{K}$). To determine the propagation velocity, the distance between the SMD board to the OST is measured to be 8.6 cm (d_f) and the measured time-of-flight is determined from the delay between the trigger of the pulse to the first drop of the signal (see Fig. 8). In Fig. 8 (a), the second sound wave is measured at 1.56 K with a time-of-flight of 4.37 ms, which yields to a second sound speed of 19.6 m/s. The calculated relative velocity error from the measurement is found to be less than 1% within the range 1.5 K to 2.17 K. The deviation of the theoretical calculated value using Eq. (1) with Bendt *et al.*'s values [8] (see Fig. 8(b)) is 0.1% when $T \leq 1.8\text{K}$, and less than 1% for $T > 1.8\text{K}$. The experimentally derived data agrees well with the theoretical expectation especially in the

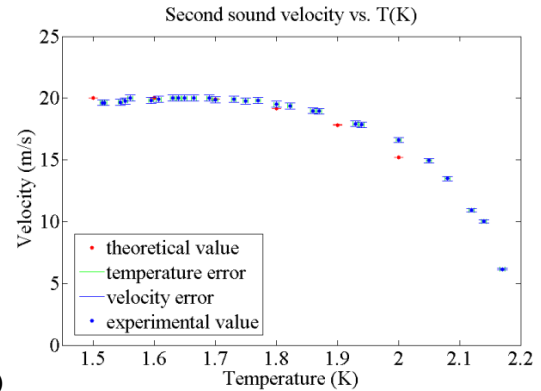
region of 1.5 K to 1.8 K. The second sound velocity along with the signal strength shown in Fig. 7 implies the importance of the helium bath temperature during the quench test. This could affect the ability to detect the signal of the OST during the occurrence of each quench event.

Distance Calculation using Second Sound Velocity

The adjustable insert is mounted with an OST which allows the distance between the SMD board and the OST (movable) to be varied. By using the measured second sound velocity, the measured time-of-flight from the OSTs and the distance (d_{cal}) between each OST and the SMD may be determined. The other OST (non-movable) is fixed at $d_f = 9.44\text{ cm}$ above the board for comparison.



(a)



(b)

Figure 8: (a) Time-of-flight is measured from the point when the pulse is triggered until the OST receives the signal. (b) Comparison of theoretically calculated [9] and experimental values of second sound velocity.

In Fig. 9, the data was taken at 1.69 K, with the movable OST adjusted to the highest position ($a = 10\text{ cm}$) in our setup, at $d_a = 19.3\text{ cm}$. The calculated distance error is less than $\pm 0.8\text{ cm}$. The difference of the measured and calculated distance ($\Delta = d_{measured} - d_{cal}$) = 1.6 cm is explained by the fact that when moving the adjustable insert during the measurement, the position of the OST/insert in the cryostat was accidentally turned. Seven measurement results performed at 1.69 K using SMD 3 are shown in Fig. 10. Fig. 10 (a) shows the reproducibility

of the second sound signal and Δ is within the range of the error bars. In Fig. 10 (b), a is varied with a step size of $\approx \pm 3$ cm starting from $a = 0$. Measurement 1 and 7 show the largest Δ , thus we would like to improve the method of adjusting the height of the OST without affecting its orientation during the measurement.

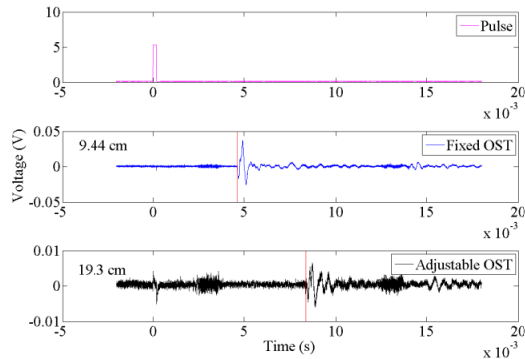
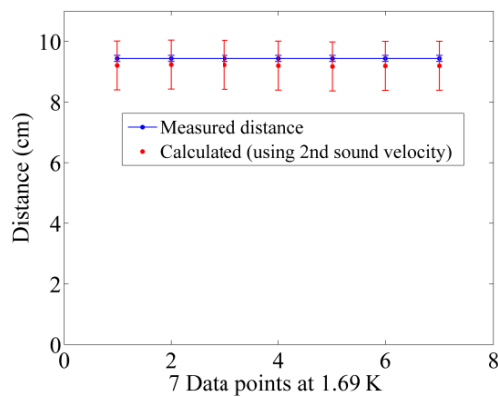
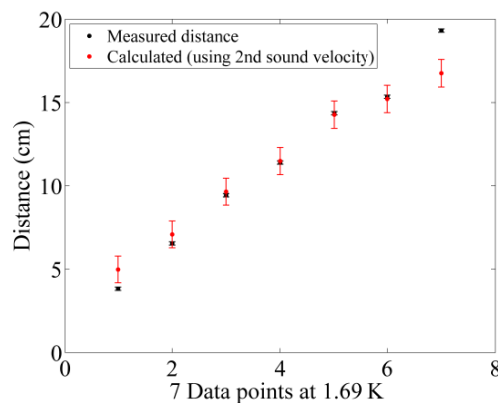


Figure 9: Second sound signal from a fixed OST and an adjustable OST. The red line indicates the arrival of the second sound. The adjustable OST situated further away from the heating source at 19.3 cm shows the time delay to the fixed OST at 9.44 cm.



(a)



(b)

Figure 10: Seven measurements taken at 1.69 K with SMD 3 as heater source. Comparison of the measured distance (d_a) and calculated distance (d_{cal}) using the measured second sound velocity as shown in Fig. 8(b) between SMD 3 and (a) fixed OST and the (b) adjustable OST.

OST MANUFACTURING

The first eight OSTs tested at CERN for the second sound measurement were received from Cornell. Recently several new OSTs have been manufactured at CERN and a study performed on the membrane sputtering process, foreseen to be used for the SPL cavity.

The manufacturing process is divided into two sections: the production of the mechanical parts and the membrane sputtering. The former contains a metallic back plate, an electrode, and a metallic upper lid; the latter results in a porous polycarbonate membrane sputtered with a layer of conductive material.

Mechanical Parts Manufacturing

The material used for producing the back plate and the upper lid is aluminium. Brass is used to make the electrode. Between the electrode and the back plate, an epoxy mix is filled. The OST manufacturing process is based on the original Cornell design [10] whereas a LEMO connector is used instead of an SMA connector. This enhances the convenience of installation.

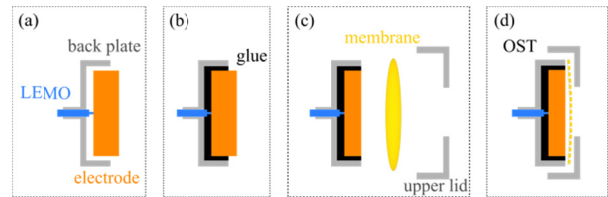


Figure 11: Schematic drawings of the manufacturing procedure.

The manufacturing process is shown in series Fig. 11. The outer ring on the LEMO connector is first removed in order to screw in the back plate with a pre-made thread. The back plate along with the LEMO connector is then to be fitted in a pre-drilled hole in the middle of the brass electrode, leaving a gap for an isolation material to go in (Fig. 11(a)). An epoxy mix with 20 parts of Stycast 2651MM and 3 parts of Catalyst 23LV is inserted into the gap (Fig. 11(b)). When the epoxy mix is solidified, the redundant part of the brass is then machined to maintain the flatness of the surface (Fig. 11(c)). A conductive porous membrane is placed on the top of the completed transducer body in order to be clamped by the upper lid (see Fig. 11(d)). Four M2 screws are used to fix the OSTs at every 90 degree on the upper lid. At the moment there are 11 OSTs with LEMO connectors at CERN.

Membrane Sputtering

A metal film is sputtered on the 25 mm diameter polycarbonate nuclearpore membranes (Whatman 110606) without covering the $0.2 \mu\text{m}$ of pores in diameter spread over the membrane. The metal film ensures the conduction of the membrane and between the back plate and the upper lid. One side of the membrane has a smooth surface, the other is rough. Fig. 12 shows a scanning electron microscopy (SEM) picture taken by LEO 430i

SEM at 5000x magnification of the smooth side of a non-sputtered membrane. The black dots indicate the nuclear pores on the membrane. The blurring of the image is caused by the accumulation of static charge on the non-conductive membrane when scanned by the electron beam. It should be noted that the sputtered layer ought to be thinner than the membrane so as to prevent blocking the pores.

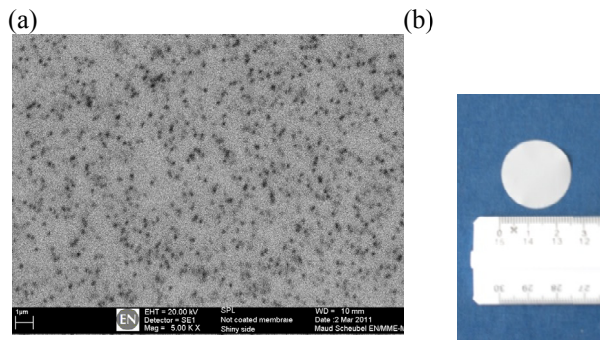


Figure 12: (a) SEM image of a non-sputtered polycarbonate membrane. The magnification is 5000x. (b) The non-sputtered membrane with 25 mm in diameter [11].

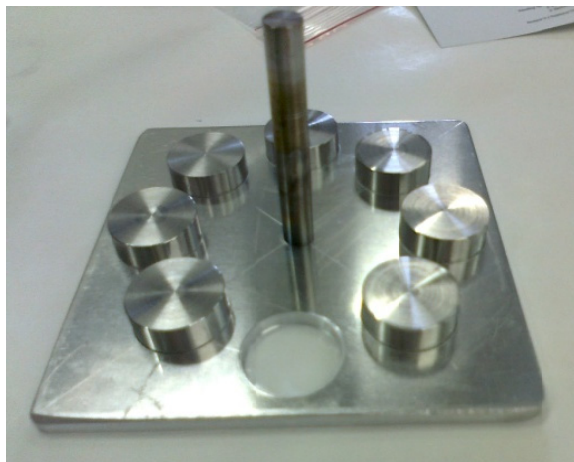


Figure 13: The membrane holder consists of eight hollow circles for placing the membranes and eight cylinder weights to secure the membranes during the sputtering process in vacuum.

A membrane holder made of stainless steel has been manufactured to allow eight membranes to be sputtered in one run (Fig. 13). The diameter of each hollow circle is 25.2 mm in order to hold the membranes, and the opening for the sputtering area is 21 mm. Stainless steel cylinders are placed on top of each hole to secure the membranes during the sputtering process. In the first sputtering test, Titanium was sputtered because of its good adherence to polycarbonate. The thickness was 90 nm which yields a more sufficient conductive layer. Nevertheless, due to this thick layer on the membrane, all membranes were curled at the moment when the cylinder is removed (see Fig. 14

(a)). Standard adherence tests, scotch test, showed good adherence of Ti film on the membranes, even after three thermal cycles of the coated membranes in liquid nitrogen were completed. An extended endurance test was done by dipping the Ti sputtered membrane into liquid nitrogen (77 K) after the previous stated processes. However a force applied manually to flatten the film results in the folds appeared on the membrane seen in Fig. 14 (b).

To avoid the curly effect of a sputtered membrane, a more conductive layer of gold (Au) was selected with a thickness of 50 nm after sputtering a thin Ti layer (3 nm) to improve the adherence of Au to polycarbonate. The curly effect is reduced (see Fig. 14 (c)) and the membrane is flattened after the endurance test in liquid nitrogen without applying any extra force as shown in Fig. 14 (d). In Fig. 15, a set of SEM image of the Ti/Au membrane and Ti membrane is presented. The Cornell supplied OSTs were tested with these new CERN Au membranes and showed reproducible second sound signal results as presented throughout this paper. Therefore another set of 16 membranes with 3 nm Ti and 50 nm Au were produced to be used in CERN-manufactured OSTs.

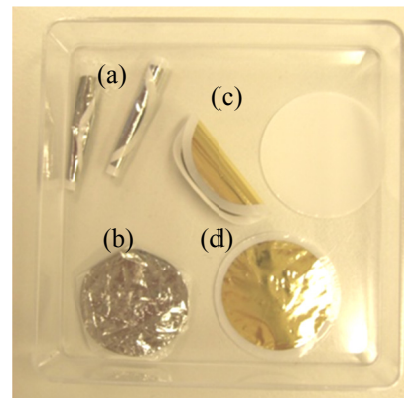


Figure 14: Five sputtered membrane and one non-sputtered membrane. (a) The curly Ti sputtered membrane with a thickness of 90 nm. (b) The Ti membrane shows folds introduced by manual force for flattening the membrane after the liquid nitrogen endurance test. (c) A less curly Au membrane came out of the sputtering holder. (d) A flat Au surface appeared after the endurance test in liquid nitrogen without extra force.

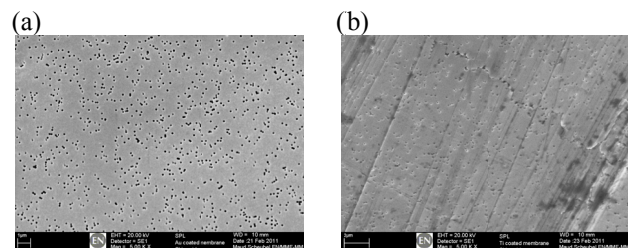


Figure 15: SEM images of the (a) Ti (3 nm)/Au (50 nm) sputtered membrane and (b) Ti sputtered membrane (90 nm). The lines in the picture show the folds on Ti membrane as described in Fig. 14(b) [11].

CONCLUSION & FUTURE WORK

The second sound detection by using oscillating superleak transducers is a direct and simple method to be used for cavity diagnostics. The study of second sound characteristics plays an indispensable role on understanding the mechanism of second sound in superfluid helium. An efficient noise reduction increases the discernment of the second sound signal to noise level (S/N). It is shown that the second sound amplitude decreased with the superfluid helium temperature and increases with the simulating heating voltage (the quench spot in a cavity).

The measured second sound velocity below the lambda point shows agreement with the theoretically predicted curve and was used to determine the distance between the OST and the heating spot. By evaluating the arrival time of the second sound signal after triggering the heater, the distance between the heater and the OST can reproducibly be determined for the fixed and the adjustable OST. The distance computed using the measured second sound velocity agrees with the manually measured results within the calculated systematic error. A more accurate method of determining the distance manually will be developed in the next test run.

Newly manufactured OSTs at CERN feature LEMO connectors and membranes sputtered with 3 nm of Ti and 50 nm of Au. Eight of these were recently installed on the SPL test cavity and it is scheduled to undergo RF test in the next months.

The Cryolab second sound test setup provides an important indicator for the cavity tests such as the operating temperature and the behaviour of the second sound wave. Thus the measurements and studies will continue to enhance the understanding of the characteristics of second sound and the OSTs.

ACKNOWLEDGEMENTS

We extend many thanks to Drs. Zack Conway, Eric Smith and Prof. Georg Hoffstaetter at Cornell University who provided their OSTs, valuable knowledge and experience.

We would also like to thank Christophe Nicou for the OST manufacturing process, Maud Scheubel for the SEM sessions and Luca Arnaudon for a lot of help in our setup and electronics devices. Last but not least, we are thankful for all the help in the Cryolab for our second sound measurements.

REFERENCES

- [1] R. Sherlock, and D. Edwards, "Oscillating Superleak Second sound Transducers", *The Review of Scientific Instruments*, **41**, 1603 (1970)
- [2] K. W. Shepard, *et al.*, "Spilt Ring Resonator For the Argonne Superconducting Heavy Ion Booster", *IEEE Trans. Nucl. Sci.* **NS-24**, 1147 (1977)
- [3] R. Wang, *et al.*, "Precision Second-Sound Velocity Measurements, *Journal of Low Temperature Physics*", **68**, 409 (1987)
- [4] Z. A. Conway, *et al.*, "ILC Testing Program at Cornell University", SRF 2009, Berlin, Germany, September 2009, TUOAAU05, 176
- [5] Z. A. Conway, *et al.*, "Defect Location in Superconducting Cavities Cooled with He-II Using Oscillating Superleak Transducers", SRF 2009, Berlin, Germany, September 2009, TUOAAU05
- [6] F. Schlander, *et al.*, "Progress on Diagnostics Tools for Superconducting High-Gradient Cavities", *Private Communication*
- [7] M. P. Kelly, *et al.*, "A Simple Second Sound Detection Technique for SRF Cavities", TUPPO032
- [8] Datasheet of thick film resistors, <http://www.niccomp.com>
- [9] P. Bendt, *et al.*, "Excitations in Liquid Helium: thermodynamic Calculations", *Physical Review*, **113**, 1386 (1959)
- [10] E. Smith, *Private Communication*
- [11] M. Scheubel, *Private Communication*